Genetic Analysis of a Metazoan Pathway using Transcriptomic Phenotypes

David Angeles-Albores[1, 2,†]   Carmie Puckett Robinson[1, 2, 3,†]   Brian A. Williams[1]

Barbara J. Wold[1]   Paul W. Sternberg[1, 2, *]

March 3, 2017

† These authors contributed equally to this work
1 Division of Biology and Biological Engineering, Caltech, Pasadena, CA, 91125, USA
2 Howard Hughes Medical Institute, Caltech, Pasadena, CA, 91125, USA
3 Department of Neurology, Keck School of Medicine, University of Southern California, Los Angeles, California, 90033, USA
* Corresponding author. Contact: pws@caltech.edu

Abstract

RNA-seq is commonly used to identify genetic modules that respond to a perturbation. Although transcriptomes have been mainly used for target gene discovery, their quantitative nature makes them attractive structures with which to study genetic interactions. To understand whether whole-organism RNA-seq is suitable for genetic pathway reconstruction, we sequenced the transcriptome of four single mutants and two double mutants of the hypoxia pathway in *C. elegans*. By comparing the expression levels of double mutants with their corresponding single mutants, we were able to determine, on a genome-wide level, that EGL-9 acts along VHL-1-dependent and independent branches to inhibit HIF-1. We were also able to observe transcriptome-wide suppression of the *egl-9(lf)* phenotype in an *egl-9(lf) hif-1(lf)* double mutant. As a by-product of our analysis, we identified a core hypoxic response consisting of 355 genes, and 45 genes that have *hif-1*-independent, *vhl-1*-dependent expression. Finally, we are able to identify 31 genes that exhibit non-canonical epistasis: for these genes, *vhl-1(lf)* mutants show opposing effects to *egl-9(lf)* mutants, but the *egl-9(lf);vhl-1(lf)* exhibits the *egl-9(lf)* phenotype. We suggest that this non-canonical epistasis reflects unexplored aspects of the hypoxia pathway. We discuss the implications, benefits and advantages of using transcriptomic phenotypes to perform pathway analysis.

Introduction

Genetic analysis of molecular pathways has traditionally been performed through epistatis analysis. Generalized epistasis indicates that two genes interact functionally; such interaction can involve the direct interaction of their products or the interaction of any consequence of their function (small molecules, physiological or behavioral effects)[1]. If two genes interact, and the mutants of these genes have a quantifiable phenotype, the double mutant of interacting genes will have a phenotype that is not the sum of the phenotypes of the single mutants that make up its genotype. Epistasis analysis remains a cornerstone of genetics today[2].

Recently, biological studies have shifted in focus from studying single genes to studying all genes in parallel. In particular, RNA-seq[3] enables biologists to identify genes that change expression in response to a perturbation. Gene expression profiling using RNA-seq has become much more sensitive thanks to deeper

1

and more frequent sequencing due to lower sequencing costs[4], better and faster abundance quantification[5,6,7], and improved differential expression analysis methods[8,9]. RNA-seq has been successfully used to identify genetic modules involved in a variety of processes, including T-cell regulation[10,11], the *Caenorhabditis elegans* (*C. elegans*) linker cell migration[12], and planarian stem cell maintenance[13,14]. For the most part, the role of transcriptional profiling has been restricted to target gene identification.

Although transcriptional profiling has been primarily used for descriptive purposes, transcriptomic phenotypes have previously been used to make genetic inferences. Microarray analyses in *S. cerevisiae* and *D. discoideum* were used to show that transcriptomes can be interpreted to infer genetic relationships in simple eukaryotes[15,16]. eQTL studies in many organisms, from yeast to humans, have established the usefulness of transcriptomic phenotypes for population genetics studies[17,18,19,20]. In cell culture, single-cell RNA-seq has seen significant progress towards using transcriptomes as phenotypes with which to test genetic interactions[21,22]. More recently, we have identified a new developmental state of *C. elegans* using whole-organism transcriptome profiling[23]. To investigate the ability of whole-organism transcriptomes to serve as quantitative phenotypes for epistasis analysis in metazoans, we sequenced the transcriptomes of of four well-characterized loss of function mutants in the *C. elegans* hypoxia pathway[24,25,26,27].

Metazoans depend on the presence of oxygen in sufficient concentrations to support aerobic metabolism. Genetic pathways evolved to rapidly respond to any acute or chronic changes in oxygen levels at the cellular or organismal level. Biochemical and genetic approaches identified the Hypoxia Inducible Factors (HIFs) as an important group of oxygen-responsive genes that are involved in a broad range of human pathologies[28].

Hypoxia Inducible Factors are highly conserved in metazoans[29]. A common mechanism for hypoxia-response induction is heterodimerization between a HIFα and a HIFβ subunit; the heterodimer then initiates transcription of target genes[30]. The number and complexity of HIFs varies throughout metazoans, with humans having three HIFα subunits and two HIFβ subunits, whereas in the roundworm *C. elegans* there is a single HIFα gene, *hif-1*[27] and a single HIFβ gene, *ahr-1*[31]. HIF target genes have been implicated in a wide variety of cellular and extracellular processes including glycolysis, extracellular matrix modification, autophagy and immunity[32,33,34,35,28].

Levels of HIFα proteins tend to be tightly regulated. Under conditions of normoxia, HIF-1α exists in the cytoplasm and partakes in a futile cycle of continuous protein production and rapid degradation[36]. HIF-1α is hydroxylated by three proline hydroxylases in humans (PHD1, PHD2 and PHD3) but is only hydroxylated by one proline hydroxylase (EGL-9) in *C. elegans*[37]. HIF-1 hydroxylation increases its binding affinity to Von Hippel Lindau Tumor Suppressor 1 (VHL-1), which allows ubiquitination of HIF-1 leading to its subsequent degradation. In *C. elegans*, EGL-9 activity is inhibited by binding of CYSL-1, and CYSL-1 activity is in turn inhibited at the protein level by RHY-1, possibly by post-translational modifications to CYSL-1[38] (see Fig. 1).

Here, we show that transcriptomes contain robust signals that can be used to infer relationships between genes in complex metazoans by reconstructing the hypoxia pathway in *C. elegans* using RNA-seq. Furthermore, we show that the phenomenon of phenotypic epistasis, a hallmark of genetic interaction, holds at the molecular systems level. We also demonstrate that transcriptomes contain sufficient information, under certain circumstances, to order genes in a pathway using only single mutants. Finally, we were able to identify genes that appear to be downstream of *egl-9* and *vhl-1*, but do not appear to be targets of *hif-1*. Using a single set of genome-wide measurements, we were able to observe and quantitatively assess significant fraction of the known transcriptional effects of *hif-1* in *C. elegans*. A complete version of the analysis, with ample documentation, is available at `https://wormlabcaltech.github.io/mprsq`.

Results

The hypoxia pathway controls thousands of genes in *C. elegans*

We selected four single mutants within the hypoxia pathway for expression profiling: *egl-9(lf)* (*sa307*), *rhy-1(lf)* (*ok1402*), *vhl-1(lf)* (*ok161*), *hif-1(lf)* (*ia4*). We also sequenced the transcriptomes of two double mutants, *egl-9(lf);vhl-1(lf)* (*sa307, ok161*) and *egl-9(lf) hif-1(lf)* (*sa307, ia4*) as well as wild-type N2 as a control sample. Each genotype was sequenced in triplicate at a depth of 15 million reads. We performed whole-organism RNA-seq of these mutants at a moderate sequencing depth ($\sim$ 7 million mapped reads for each individual replicate) under normoxic conditions. For single samples, we identified around 22,000
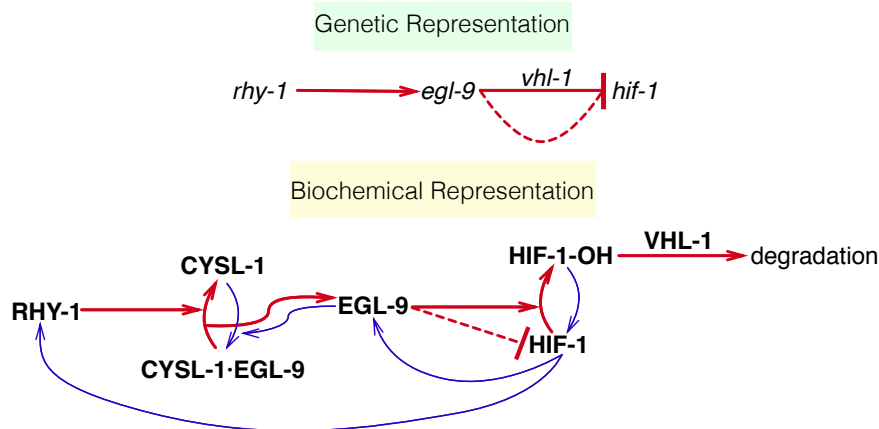
Figure 1. Genetic and biochemical representation of the hypoxia pathway in *C. elegans*. Red arrows are arrows that lead to inhibition of HIF-1, and blue arrows are arrows that increase HIF-1 activity or are the result of HIF-1 activity. EGL-9 is known to exert *vhl-1*-dependent and independent repression on HIF-1 as shown in the genetic diagram. The *vhl-1*-independent repression of HIF-1 by EGL-9 is denoted by a dashed line and is not dependent on the hydroxylating activity of EGL-9. Technically, RHY-1 inhibits CYSL-1, which in turn inhibits EGL-9, but this interaction was abbreviated in the genetic diagram for clarity.

different isoforms per sample, which allowed us to measure differential expression of 18,344 isoforms across all replicates and genotypes (this constitutes ∼70% of the protein coding isoforms in *C. elegans*). We also included in our analysis a *fog-2(lf)* (*q71*) mutant which we have previously studied[23], because *fog-2* is not reported to interact with the hypoxia pathway. We analyzed our data using a general linear model on logarithm-transformed counts. Changes in gene expression are reflected in the regression coefficient, β which is specific to each isoform within a genotype. Statistical significance is achieved when the q-values for each β (p-values adjusted for multiple testing) are less than 0.1. Genes that are significantly altered between wild-type and a given mutant have β values that are statistically significantly different from 0. These coefficients are not equal to the average log-fold change per gene, although they are loosely related to this quantity. Larger magnitudes of β correspond to larger perturbations. These coefficients can be used to study the RNA-seq data in question.

In spite of the moderate sequencing depth, transcriptome profiling of the hypoxia pathway revealed that this pathway controls thousands of genes in *C. elegans*. The *egl-9(lf)* transcriptome showed differential expression of 1,806 genes. Similarly, 2,103 genes were differentially expressed in *rhy-1(lf)* mutants. The *vhl-1(lf)* transcriptome showed considerably fewer differentially expressed genes (689), possibly because it is a weaker controller of *hif-1(lf)* than *egl-9(lf)*[26]. The *egl-9(lf);vhl-1(lf)* double mutant transcriptome showed 2,376 differentially expressed genes. The *hif-1(lf)* mutant also showed a transcriptomic phenotype involving 546 genes. The *egl-9(lf) hif-1(lf)* double mutant showed a similar number of genes with altered expression (404 genes, see Table 1).

Genotype	Differentially Expressed Genes
egl-9(lf)	1,806
rhy-1(lf)	2,103
vhl-1(lf)	689
egl-9(lf);vhl-1(lf)	2,376
egl-9(lf) hif-1(lf)	404
fog-2(lf)	2090

Table 1. Number of differentially expressed genes in each mutant.

Principal Component Analysis visualizes epistatic relationships between genotypes

Principal Component Analysis (PCA) is a well-known technique in bioinformatics that is used to identify relationships between high dimensional data points[39] We performed PCA on our data to examine whether each genotype clustered in a biologically relevant manner. PCA identifies the vector that can explain most of the variation in the data;this is called the first PCA dimension. Using PCA, one can identify the first n dimensions that can explain more than 95% of the variation in the data. Sample clustering in these n dimensions often indicates biological relationships between the data, although interpreting PCA dimensions can be difficult.

After applying PCA, we expected *hif-1(lf)* to cluster near *egl-9(lf) hif-1(lf)*, because *hif-1(lf)* exhibits no phenotypic defects under normoxic conditions, in contrast to *egl-9(lf)*, which exhibits an egg-laying (Egl) phenotype in the same environment. In *egl-9(lf) hif-1(lf)* mutants the Egl phenotype of *egl-9(lf)* mutants is suppressed and instead the grossly wild-type phenotype of *hif-1(lf)* is observed. On the other hand, we expected *egl-9(lf)*, *rhy-1(lf)*, *vhl-1(lf)* and *egl-9(lf);vhl-1(lf)* to form a separate cluster since each of these genotypes is Egl and has a constitutive hypoxic response. Finally, we included as a negative control a *fog-2(lf)* mutant we have analyzed previously[23]. This data was obtained at a different time from the other genotypes, so we included a batch-normalization term in our equations to account for this. Since *fog-2* has not been described to interact with the hypoxia pathway, we expected that it should appear far away from either cluster.

The first dimension of the PCA analysis was able to discriminate between mutants that have constitutive high levels of HIF-1 and mutants that have no HIF-1, whereas the second dimension was able to discriminate between mutants within the hypoxia pathway and outside the hypoxia pathway (see Fig. 2). Therefore expression profiling measures enough signal to cluster genes in a meaningful manner in complex metazoans.
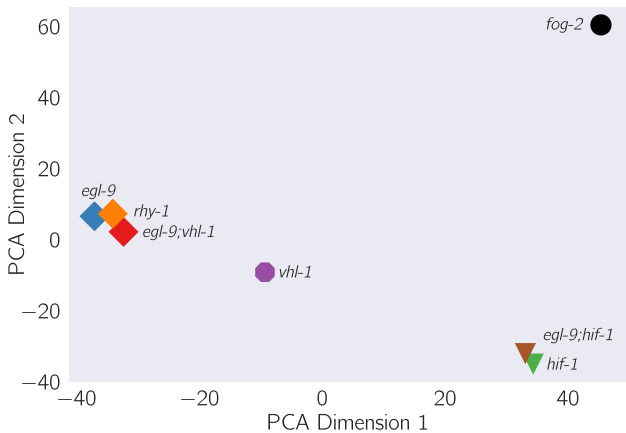

Figure 2. Principal component analysis of various *C. elegans* mutants. Genotypes that have an activated hypoxia response (*i.e*, *egl-9(lf)*, *vhl-1(lf)*, and *rhy-1(lf)*) cluster far from *hif-1(lf)*. *hif-1(lf)* clusters with the suppressed *egl-9(lf) hif-1(lf)* double mutant. The *fog-2(lf)* transcriptome, used as an outgroup, is far away from either cluster.

Reconstruction of the hypoxia pathway from first genetic principles

Having shown that the signal in the mutants we selected was sufficient to cluster mutants using the values of the regression coefficients β, we set out to reconstruct the hypoxia pathway from genetic first principles. In general, to reconstruct a pathway, we must first assess whether two genes act on the same phenotype. If they do not act on the same phenotype (the set of commonly differentially regulated genes between two mutants is empty), these mutants are independent. If they are not independent, then two mutants have a shared transcriptomic phenotype (STP)—a set of genes or isoforms that are differentially expressed in both mutants, without taking into account what direction they change in. In this case, we must measure whether these genes act additively or epistatically on the measured phenotype; if there is epistasis we must measure

whether it is positive or negative, in order to assess whether the epistatic relationship is a genetic suppression   141
or a synthetic interaction.   142

Genes in the hypoxia mutant act on the same transcriptional phenotype   143

We observed that all the hypoxia mutants had significant shared transcriptomic phenotypes (fraction of the   144
transcriptomes that was shared between mutants ranged from a minimum of 6.8% shared between *hif-1(lf)*   145
and *egl-9(lf);vhl-1(lf)* to a maximum of 31% shared genes between *egl-9(lf)* and *egl-9(lf);vhl-1(lf)*). For   146
comparison, we also analyzed a previously published *fog-2(lf)* transcriptome[23]. The *fog-2* gene is involved   147
in masculinization of the *C. elegans* germline, which enables sperm formation, and is not known to be   148
involved in the hypoxia pathway. The hypoxia pathway mutants and the *fog-2(lf)* mutant also showed   149
shared transcriptomic phenotypes (3.6%–12% genes), but correlations between expression level changes were   150
considerably weaker (see below), suggesting that there is minor cross-talk between these pathways.   151
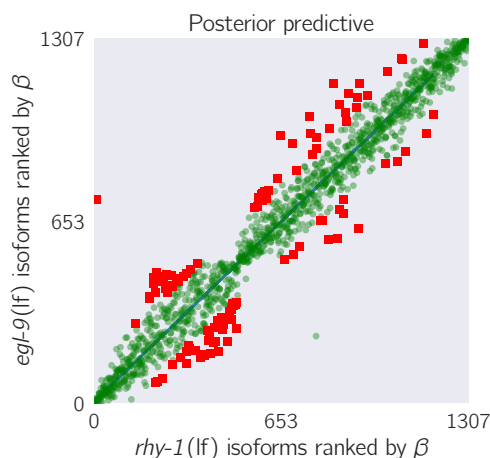

Figure 3. Strong transcriptional correlations can be identified between genes that share a positive regulatory
connection. We took the *egl-9(lf)* and the *rhy-1(lf)* transcriptomes, identified differentially expressed genes
common to both transcriptomes and ranked each gene according to its differential expression coefficient β.
We plotted the rank of each gene in *rhy-1(lf)* versus the rank of the same gene in the *egl-9(lf)* transcriptome.
The result is an almost perfect correlation. Green, transparent large points mark inliers to the primary
regressions (blue lines); red squares mark outliers to the primary regressions.

We wanted to know whether it was informative to look at quantitative agreement within STPs. For   152
each mutant pair, we rank-transformed the regression coefficients β of each isoform within the STP, and   153
calculated lines of best fit using Bayesian regression with a Student-T distribution to mitigate noise from   154
outliers and plotted the results in a rank plot (see Fig 3). For transcriptomes associated with the hypoxia   155
pathway, we found that these correlations tended to have values higher than 0.9 with a tight distribution   156
around the line of best fit. The correlations for mutants from the hypoxia pathway with the *fog-2(lf)* mutant   157
were considerably weaker, with magnitudes between 0.6–0.85 and greater variance around the line of best   158
fit. Although *hif-1* is known to be genetically repressed by *egl-9*, *rhy-1* and *vhl-1*[24,25], all the correlations   159
between mutants of these genes and *hif-1(lf)* were positive.   160

After we calculated the pairwise correlation within each STP, we weighted the result of each regression by   161
the number of isoforms within the STP and divided by the total number of differentially expressed isoforms   162
present in the two mutant transcriptomes that contributed to that specific STP, $N_{\mathrm{overlap}}/N_{\mathrm{g_1 \cup g2}}$. The   163
weighted regressions recapitulated a module network (see Fig. 4). We identified a strong positive interaction   164
between *egl-9(lf)* and *rhy-1(lf)*. The magnitude of this weighted correlation derives from the magnitude   165
of the transcriptomes for these mutants (1,806 and 2,103 differentially expressed genes respectively) and   166
the overlap between both genes was extensive, which makes the weighting factor considerably larger than   167
other pairs. The weak correlation between *hif-1(lf)* and *egl-9(lf)* results from the small size of the *hif-1(lf)*   168
transcriptome and the small overlap between the transcriptomes.   169

The fine-grained nature of transcriptional phenotypes means that these weighted correlations between transcriptomes of single mutants are predictive of genetic interaction.
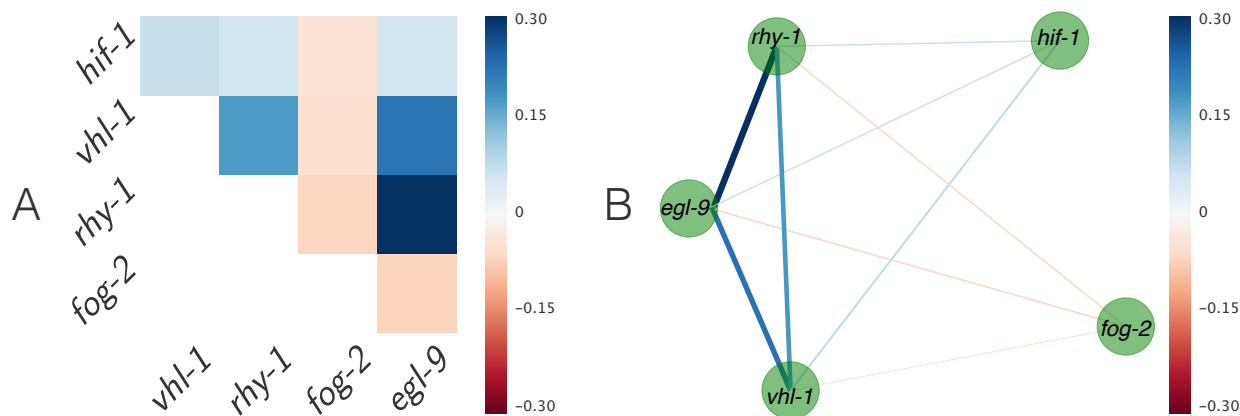

Figure 4. **A**. Heatmap showing pairwise regression values between all single mutants. **B**. Correlation network drawn from **A**. Edge width is proportional to the logarithm of the magnitude of the weighted correlation between two nodes divided by absolute value of the weighted correlation value of smallest magnitude. Edges are also colored according to the heatmap in **A**. Inhibitors of *hif-1* are tightly correlated and form a control module; *hif-1* is positively correlated to its inhibitors, albeit weakly; and *fog-2*, a gene that is not reported to interact with the hypoxia pathway, has the smallest, negative correlation to any gene.

A quality check of the transcriptomic data reveals excellent agreement with the literature

One way to establish whether genes are acting additively or epistatically to each other is to perform qPCR of a reporter gene in the single and double mutants. This approach was used to successfully map the relationships within the hypoxia pathway (see, for example[26,25]). A commonly used hypoxia reporter gene is *nhr-57*, which is known to exhibit a several-fold increase in mRNA expression when HIF-1 accumulates[25,34,40]. Likewise, increased HIF-1 fucntion is known to cause increased of *rhy-1* and *egl-9*[41].

We can selectively look at the expression of a few genes at a time. Therefore, we queried the changes in expression of *rhy-1*, *egl-9*, and *nhr-57*. We included the nuclear laminin gene *lam-3* as a representative negative control not believed to be responsive to alterations in the hypoxia pathway. *nhr-57* was upregulated in *egl-9(lf)*, *rhy-1(lf)* and *vhl-1(lf)*, but remains unchanged in *hif-1(lf)*. *egl-9(lf);vhl-1(lf)* had an expression level similar to *egl-9(lf)*; whereas the *egl-9(lf) hif-1(lf)* mutant showed wild-type levels of the reporter expression, as reported previously[25] (see Fig. 5).

We observed changes in *rhy-1(lf)* expression consistent with previous literature[25] when HIF-1 accumulates. We also observed increases in *egl-9* expression in *egl-9(lf)*. *egl-9* is known as a hypoxia responsive gene[41]. Although changes in *egl-9* expression were not statistically significantly different from the wild-type in *rhy-1(lf)* and *vhl-1(lf)* mutants, the mRNA levels of *egl-9* still trended towards increased expression in these genotypes. As with *nhr-57*, *egl-9* and *rhy-1* expression were wild-type in *egl-9(lf) hif-1(lf)* and *egl-9(lf);vhl-1(lf)* mutant showed expression phenotypes identical to *egl-9(lf)*. This dataset also showed that knockout of *hif-1* resulted in a modest increase in the levels of *rhy-1*. This suggests that *hif-1*, in addition to being a positive regulator of *rhy-1*, also inhibits it, which constitutes a novel observation. Using a single reporter we would have been able to reconstruct an important fraction of the genetic relationships between the genes in the hypoxia pathway—-but would likely fail to observe yet other genetic interactions, such as the evidence for *hif-1* negatively regulating *rhy-1* transcript levels.

Transcriptome-wide epistasis

Ideally, any measurement of transcriptome-wide epistasis should conform to certain expectations. First, it should make use of the regression coefficients of as many genes as possible. Second, it should be summarizable
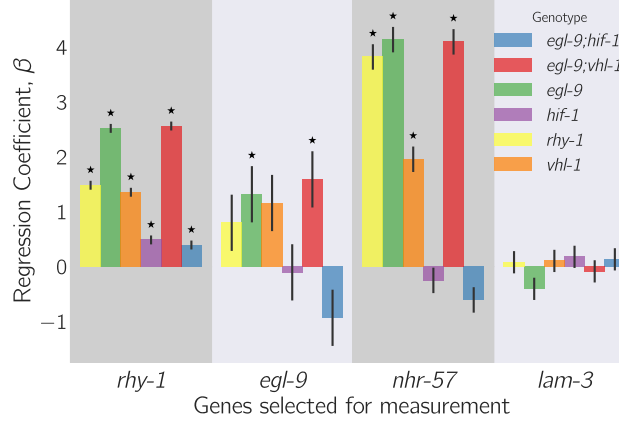
Figure 5. Top: Observed β values of select genes. We selected four genes (*rhy-1*, *egl-9*, *nhr-57* and *lam-3*, shown on the x-axis) and plotted their regression coefficients, β, as measured for every genotype (represented by one of six colors) to study the epistatic relationships between each gene. Asterisks above a bar represent a regression coefficient statistically significantly different from 0 ($q < 10^{-1}$) relative to a wild-type control. Error bars show standard error of the mean value of β. *nhr-57* is an expression reporter that has been used previously to identify *hif-1* regulators[25,26]. *lam-3* is shown here as a negative control that should not be altered by mutations in this pathway. We measured modest increases in the levels of *rhy-1* mRNA when *hif-1(lf)* is knocked out.

in a single, well-defined number. Third, it should have an intuitive behavior, such that special values of the statistic should each have an unambiguous interpretation.

One way of displaying transcriptome-wide epistasis is to plot transcriptome data onto an epistasis plot (see Fig 6). In an epistasis plot, the X-axis represents the expected expression of a double mutant a^-b^- if a and b interact additively. In other words, each individual isoform's x-coordinate is the sum of the regression coefficients from the single mutants a^- and b^-. The Y-axis represents the deviations from the additive (null) model, and can be calculated as the difference between the observed regression coefficient and the predicted regression coefficient. Only genes that are differentially expressed in all three genotypes are plotted. Assuming that the two genes interact via a simple phenotype (for example, if both genes affect a transcription factor that generates the entire transcriptome), these plots will generate specific patterns that can be described through linear regressions. The slope of these lines, $s_{a,b}$, is the transcriptome-wide epistasis coefficient.

Epistasis plots can be understood intuitively for simple cases of genetic interactions. If two genes act additively on the same set of differentially expressed isoforms then all the plotted points will fall along the line $y = 0$. If two genes interact in an unbranched pathway, then a^- and b^- should have identical phenotypes for a^-, b^- and a^-b^-, if all the genotypes are homozygous for genetic null alleles[1]. It follows that the data points should fall along a line with slope equal to $-\frac{1}{2}$. On the other hand, in the limit of complete inhibition of a by b, the plots should show a line of best fit with slope equal to -1[1]. Genes that interact synthetically (*i.e.*, through an OR-gate) will fall along lines with slopes > 0. When there is epistasis of one gene over another, the points will fall along a line of best fit with slope $s_{ab=b}$ or $s_{ab=a}$. This slope must be determined from the single-mutant data. From this information, we can use the single mutant data to predict the distribution of slopes that results for each case stated above, as well as for each epistatic combination ($a^-b^- = a^-$ or $a^-b^- = b^-$). The transcriptome-wide epistasis coefficient ($s_{a,b}$), emerges as a powerful way to quantify epistasis because it integrates information from many different genes or isoforms into a single number (see Fig. 6).

In our experiment, we studied two double mutants, *egl-9(lf) hif-1(lf)* and *egl-9(lf);vhl-1(lf)*. We wanted to understand how well an epistasis analysis based on transcriptome-wide coefficients agreed with the epistasis results reported in the literature, which were based on qPCR of single genes. Therefore, we performed orthogonal distance regression on the two gene combinations we studied (*egl-9* and *vhl-1*; and *egl-9* and *hif-1*) to determine the epistasis coefficient for each gene pair. We also generated models for the special cases

---

[1]Specifically, this follows from assuming that b^- is wild-type under the conditions assayed; and $a^-b^- = b^- =$ wild-type

mentioned above (additivity, $a^-b^- = a^-$, strong suppression, etc. . .) using the single mutant data. For every simulation, as well as for the observed data, we used bootstraps to generate probability distributions of the epistasis coefficients.

When we compared the predictions for the transcriptome-wide epistasis coefficient, $s_{egl-9,vhl-1}$ under different assumptions with the observed slope (-0.42). We observed that the predicted slope matched the simulated slope for the case where *egl-9* is epistatic over *vhl-1* (*egl-9(lf) = egl-9(lf);vhl-1(lf)*, see Fig. 6) and did not overlap with any other prediction. Next, we predicted the distribution of $s_{egl-9,hif-1}$ for different pathways and contrasted with the observed slope. In this case, we saw that the uncertainty in the observed coefficient overlapped significantly with the strong suppression model, where EGL-9 strongly suppresses HIF-1, and also with the model where *hif-1(lf) = egl-9(lf) hif-1(lf)*. In this case, both models are reasonable—HIF-1 is strongly suppressed by EGL-9, and we know from previous literature that the epistatic relationship, *hif-1(lf) = egl-9(lf) hif-1(lf)*, is true for these mutants. In fact, as the repression of HIF-1 by EGL-9 becomes stronger, the epistatic model should converge on the limit of strong repression (see Epistasis).

Another way to test which model best explains the epistatic relationship between *egl-9* and *vhl-1* is to use Bayesian model selection to calculate an odds ratio between two models to explain the observed data. Models can be placed into two categories: parameter-free and fit. Parameter free models are 'simpler' because their parameter space is smaller (0 parameters) than the fit models (*n* parameters). By Occam's razor, simpler models should be preferred to more complicated models. However, simple models suffer from the drawback that systematic deviations from them cannot be explained or accomodated, whereas more complicated models can alter the fit values to maximize their explanatory power. In this sense, more complicated models should be preferred when the data shows systematic deviations from the simple model. Odds-ratio selection gives us a way to quantify the trade-off between simplicity and explanatory power.

We reasoned that comparing a fit model ($y = \alpha \cdot x$, where α is the slope of best fit) against a parameter-free model ($y = \gamma \cdot x$, where γ is a single number) constituted a conservative approach towards selecting which theoretical model (if any) best explained the data. In particular, this approach will tend to strongly favor the line of best fit over simpler model for all but very small, non-systematic deviations. We decided that we would reject the theoretical models only if the line of best-fit was 10^3 times more likely than the theoretical models (odds ratio, OR $> 10^3$). Comparing the odds-ratio between the line of best fit and the different pathway models for *egl-9* and *vhl-1* showed similar results to the simulation. Only the theoretical model *egl-9(lf) = egl-9(lf);vhl-1(lf)* could not be rejected (OR = 0.46), whereas all other models were significantly less likely than the line of best fit (OR $> 10^{44}$). Therefore, *egl-9* is epistatic to *vhl-1*. Moreover, since $s_{egl-9,vhl-1}$ is strictly between and not equal to 0 and -0.5, we conclude that *egl-9* acts on its transcriptomic phenotype in *vhl-1*-dependent and independent manners. A branched pathway that can lead to epistasis coefficients in this range is a pathway where *egl-9* interacts with its transcriptomic phenotype via branches that have the same valence (both positive or both negative)[26]. When we performed a similar analysis to establish the epistatic relationship between *egl-9* and *hif-1*, we observed that the best alternative to a free-fit model was a model where *hif-1* is epistatic over *egl-9* (OR= 2551), but the free-fit model was still preferred. All other models were strongly rejected (OR $> 10^{25}$).

Epistasis can be predicted

Given our success in measuring epistasis coefficients, we wanted to know whether we could predict the epistasis coefficient between *egl-9* and *vhl-1* in the absence of the *egl-9(lf)* genotype. Since RHY-1 indirectly activates EGL-9, the *rhy-1(lf)* transcriptome should contain more or less equivalent information to the *egl-9(lf)* transcriptome. Therefore, we generated predictions of the epistasis coefficient between *egl-9* and *vhl-1* by substituting in the *rhy-1(lf)* data. We predicted $s_{rhy-1,vhl-1} = -0.45$. Similarly, we used the *egl-9(lf);vhl-1(lf)* double mutant to measure the epistasis coefficient while replacing the *egl-9(lf)* dataset with the *rhy-1(lf)* dataset. We found that the epistasis coefficient using this substitution was -0.40. This coefficient was different from -0.50 (OR $> 10^{62}$), reflecting the same qualitative conclusion that the hypoxia pathway is branched. In conclusion, we were able to obtain a quantitatively close prediction of the epistasis coefficient for two mutants using the transcriptome of a related, upstream mutant. Finally, we showed that in the absence of a single mutant, an upstream locus can under some circumstances be used to estimate epistasis between two genes.
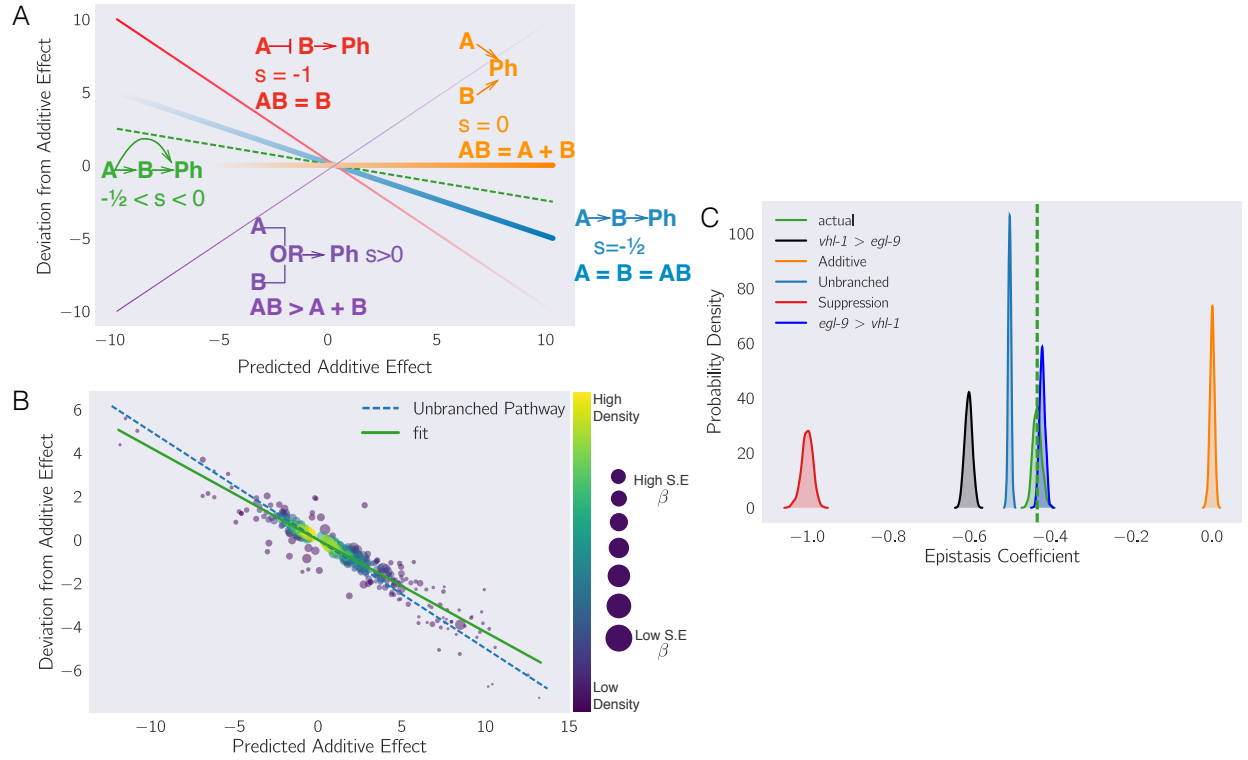
Figure 6. (**A**) Schematic diagram of an epistasis plot. The X-axis on an epistasis plot is the expected coefficient for a double mutant under an additive model (null model). The Y-axis plots deviations from this model. Double mutants that deviate in a systematic manner from the null model exhibit transcriptome-wide epistasis (s). To measure s, we perform a linear regression on the data. The slope of the line of best fit is s. This coefficient is related to genetic architectures. Genes that act additively on a phenotype (**Ph**) will have $s = 0$ (orange line); whereas genes that act along an unbranched pathway will have $s = -1/2$ (blue line). Strong repression is reflected by $s = -1$ (red line). Cases where $s > 0$ correspond to synthetic interactions (purple line), and in the limit as $s \to \infty$, the synthetic interaction must be an OR-gate. Cases where $0 < s < -1/2$ correspond to circuits that have multiple positive branches; whereas cases where $-1/2 < s < -1$ correspond to cases where the branches have different valence. Cases where $s < -1$ represent inhibitory branches. (**B**) Epistasis plot showing that the *egl-9(lf);vhl-1(lf)* transcriptome deviates significantly from a null additive. Points are colored qualitatively according to density (purple—low, yellow—high) and size is inversely proportional to the standard error (S.E.) of the y-axis (larger points, higher accuracy). The purple line is the line of best fit from an orthogonal distance regression. (**C**) Comparison of simulated epistatic coefficients against the observed coefficient. Green curve shows the bootstrapped observed transcriptome-wide epistasis coefficient for *egl-9* and *vhl-1*. Dashed green line shows the mean value of the data. Using the single mutants, we simulated coefficient distributions for a linear model (light blue, centered at -0.5); an additive model (orange, centered at 0); a model where either *egl-9* or *vhl-1* masks the other phenotype (dark blue and black, respectively) and a complete suppression model (red, centered at -1). The observed coefficient overlaps the predicted epistasis curve for *egl-9(lf);vhl-1(lf) = egl-9(lf)* (green and dark blue).

Transcriptomic decorrelation can be used to infer functional distance

So far, we have shown that RNA-seq can accurately measure genetic interactions. However, genetic interac- 281
tions are far removed from biochemical interactions: Genetic interactions do not require two gene products 282
to interact physically, nor even to be physically close to each other. RNA-seq cannot measure physical 283
interactions between genes, but we wondered whether expression profiling contains sufficient information to 284
order genes along a pathway. 285

Single genes are often regulated by multiple independent sources. The connection between two nodes 286
can in theory be characterized by the strength of the edges connecting them (the thickness of the edge); 287
the sources that regulate both nodes (the fraction of inputs common to both nodes); and the genes that 288
are regulated by both nodes (the fraction of outputs that are common to both nodes). In other words, we 289
expected that expression profiles associated with a pathway would respond quantitatively to quantitative 290
changes in activity of the pathway. Targeting a pathway at multiple points would lead to expression pro- 291
file divergence as we compare nodes that are separated by more degrees of freedom, reflecting the flux in 292
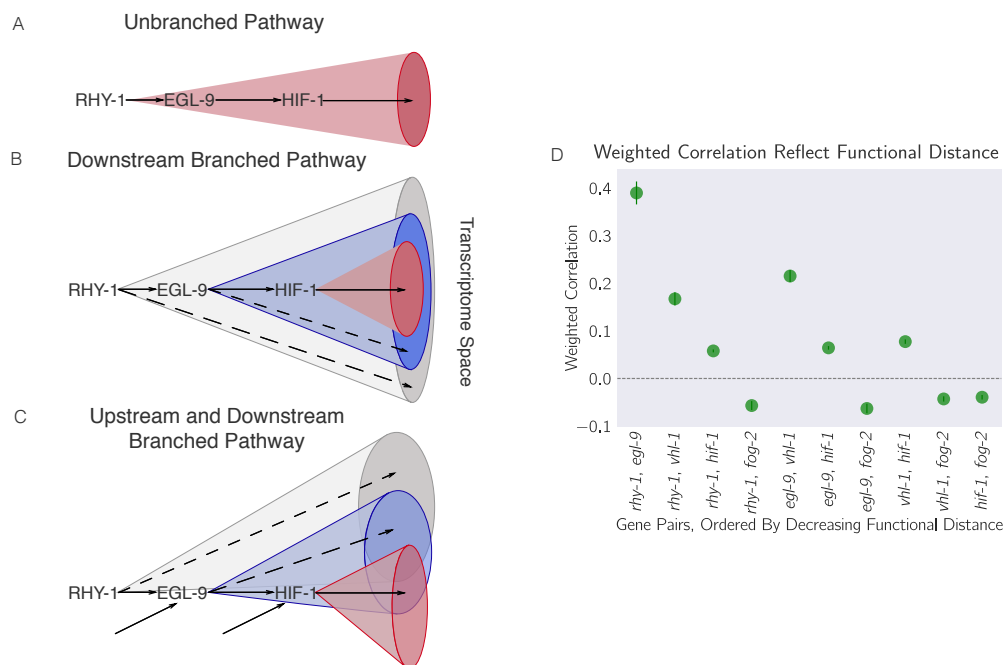information between them. 293

Figure 7. Theoretically, transcriptomes can be used to order genes in a pathway under certain assumptions.
Arrows in the diagrams above are intended to show the direction of flow, and do not indicate valence. **A**.
A linear pathway in which *rhy-1* is the only gene controlling *egl-9*, which in turn controls *hif-1* does not
contain information to infer the order between genes. **B**. If *rhy-1* and *egl-9* have transcriptomic effects that
are separable from *hif-1*, then the *rhy-1* transcriptome should contain contributions from *egl-9*, *hif-1* and
egl-9- and *hif-1*-independent pathways. This pathway contains enough information to infer order. **C**. If a
pathway is branched both upstream and downstream, transcriptomes will show even faster decorrelation.
Nodes that are separated by many edges may begin to behave almost independently of each other with
marginal transcriptomic overlap or correlation. **D**. The hypoxia pathway can be ordered. We hypothesize
the rapid decay in correlation is due to a mixture of upstream and downstream branching that happens
along this pathway. Bars show the standard error of the weighted coefficient from the Monte Carlo Markov
Chain computations.

We investigated the possibility that transcriptomic signals do in fact contain relevant information about 294
the degrees of separation by weighting the robust Bayesian regression between each pair of genotypes by the 295
size of the shared transcriptomic phenotype of each pair divided by the total number of isoforms differentially 296
expressed in either mutant ($N_{\text{Intersection}}/N_{\text{Union}}$). We plotted the weighted correlation of each gene pair, 297
ordered by increasing functional distance (see Fig. 7). In every case, we see that the weighted correlation 298

decreases monotonically due mainly, but not exclusively, to a smaller STP. We believe that this result is not due to random noise or insufficiently deep sequencing. Instead, we propose a framework in which every gene is regulated by multiple different molecular species, which induces progressive decorrelation. This decorrelation in turn has two consequences. First, decorrelation within a pathway implies that two nodes may be almost independent of each other if the functional distance between them is large. Second, it may be possible to use decorrelation dynamics to infer gene order in a branching pathway, as we have done with the hypoxia pathway.

The circuit topology of the hypoxia pathway explains patterns in the data

We noticed that while some of the rank plots contained a clear positive correlation (see Fig. 3), other rank plots showed a discernible cross-pattern (see Fig. 8). In particular, this cross-pattern emerged between *vhl-1(lf)* and *rhy-1(lf)* or between *vhl-1(lf)* and *egl-9(lf)*, even though genetically *vhl-1*, *rhy-1* and *egl-9* are all inhibitors of *hif-1(lf)*. Such cross-patterns could be indicative of feedback loops or other complex interaction patterns.
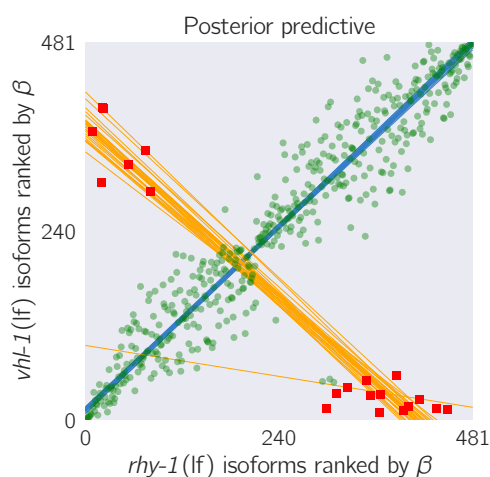

Figure 8. A feedback loop can generate transcriptomes that are both correlated and anti-correlated. The *vhl-1(lf)*/*rhy-1(lf)* STP shows a cross-pattern. Green large points are inliers to the first regression. Red squares are outliers to the first regression. Only the red small points were used for the secondary regression. Blue lines are representative samples of the primary bootstrapped regression lines. Orange lines are representative samples of the secondary bootstrapped regression lines.

If the above is correct, then it should be possible to identify *egl-9*-independent, *rhy-1(lf)*-dependent target genes in a logically consistent way. One erroneous way to identify these targets is via subtractive logic. Using subtractive logic, we would identify genes that are differentially expressed in *rhy-1(lf)* mutants but not in *egl-9(lf)* mutants. Such a gene set would consist of almost 700 genes. One major drawback of subtractive logic is that it cannot be applied when feedback loops exist between the genes in question. Another problem is that the set of identified genes are statistically indistinguishable from false positive and false negative hits because they have no distinguishing property beyond the condition that they should be differentially expressed in one mutant but not the other. In fact, this is exactly the behavior expected of false-positive or false-negative hits—presence in one, but not multiple, mutants. We need to consider the relationship between two genes before we can begin to identify targets which expression is dependent on one gene and independent of the other.

rhy-1 and *egl-9* share a well-defined relationship. RHY-1 inhibits CYSL-1, which in turn inhibits EGL-9[38]. Therefore, loss of RHY-1 leads to inactivation of EGL-9, which leads to increase in the cellular levels of HIF-1. HIF-1 in turn causes the mRNA levels of *rhy-1* and *egl-9* to increase, as they are involved in the *hif-1*-dependent hypoxia response. However, since *rhy-1* has been mutated, the observed transcriptome is RHY-1 'null'; EGL-9 'null'; HIF-1 'on'. The situation is similar for *egl-9(lf)*, except that RHY-1 is not inactive, and therefore the observed transcriptome is the result of RHY-1 'up'; EGL-9 'null'; and HIF-1 'on'.

From this pattern, we conclude that the *egl-9(lf)* and *rhy-1(lf)* transcriptomes should exhibit a cross-pattern 329
when plotted against each other: The positive arm of the cross is the result of the EGL-9 'null'; HIF-1 'on' 330
dynamics; and the negative arm reflects the different direction of RHY-1 activity between transcriptomes. 331
No negative arm is visible (with the exception of two outliers, which are annotated as pseudogenes in 332
WormBase). Therefore, in this dataset we do not find genes that have *egl-9* independent, *rhy-1*-dependent 333
expression patterns. 334

We also identified a main hypoxia response induced by disinhibiting *hif-1* (355 genes) by identifying genes 335
that were commonly up-regulated amongst *egl-9(lf)*, *rhy-1(lf)* and *vhl-1(lf)* mutants. Although the hypoxic 336
response is likely to involve between three and seven times more genes (assuming the *rhy-1(lf)* transcriptome 337
reflects the maximal hypoxic response), this is a conservative estimate that minimizes false positive results, 338
since these changes were identified in four different genotypes with three replicates each. This response 339
included five transcription factors (*W02D7.6*, *nhr-57*, *ztf-18*, *nhr-135* and *dmd-9*). The full list of genes 340
associated with the hypoxia response can be found in the Supplementary Table 1. 341

hif-1-independent effects of *egl-9* have been reported previously [40], which led us to question whether we 342
could identify similar effects in our dataset. We have observed that *hif-1(lf)* displays a modest increase in the 343
transcription of *rhy-1*, from which we speculated that EGL-9 would have increased activity in the *hif-1(lf)* 344
mutant compared to the wild-type. Therefore, we searched for genes that were regulated in an opposite 345
manner between *hif-1(lf)* and *egl-9(lf) hif-1(lf)*, and that were regulated in the same direction between all 346
egl-9(lf) genotypes. We did not find any genes that met these conditions. 347

We also searched for genes with *hif-1* independent, *vhl-1*-dependent gene expression and found 45 genes, 348
which can be found in the Supplementary Table 2. Finally, we searched for candidates directly regulated 349
by *hif-1*. Initially, we searched for genes that had were significantly altered in *hif-1(lf)* genotypes in one 350
direction, but altered in the opposite direction in mutants that activate the HIF-1 response. Only two genes 351
(*R08E5.3*, and *nit-1*) met these conditions. This could reflect the fact that HIF-1 exists at very low levels in 352
C. elegans, so loss of function mutations in *hif-1* might only have mild effects on its transcriptional targets. 353
We reasoned that genes that are overexpressed in mutants that induce the HIF-1 response would be enriched 354
for genes that are direct candidates. We found 195 genes which have consistently increased expression in 355
mutants with a constitutive hypoxic response. These genes can be found in the Supplementary Table 3. 356

Enrichment analysis of the hypoxia response 357

To validate that our transcriptomes were correct, and to understand how functionalities may vary be- 358
tween them, we subjected each decoupled response to enrichment analysis using the WormBase Enrichment 359
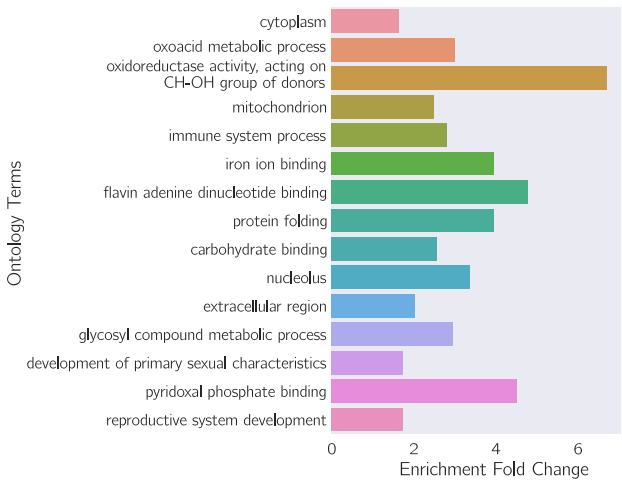Suite [42,43]. 360

Figure 9. Gene ontology enrichment analysis of genes associated with the main hypoxia response. A
number of terms reflecting catabolism and bioenergetics are enriched.

We used gene ontology enrichment analysis (GEA) on the main hypoxia response program. This showed 361
that the terms 'oxoacid metabolic process' ($q < 10^{-4}$, 3.0 fold-change, 24 genes), 'iron ion binding' ($q <$ 362

10^{-2}, 3.8 fold-change, 10 genes), and 'immune system process' ($q < 10^{-3}$, 2.9 fold-change, 20 genes) were significantly enriched. GEA also showed enrichment of the term 'mitochondrion' ($q < 10^{-3}$, 2.5 fold-change, 29 genes) (see Fig. 9). Indeed, *hif-1(lf)* has been implicated in all of these biological and molecular functions[44,45,46,47]. As benchmark on the quality of our data, we selected a set of 22 genes known to be responsive to HIF-1 levels from the literature and asked whether these genes were present in our hypoxia response list. We found 8/22 known genes, which constitutes a statistically significant result ($p < 10^{10}$). The small number of reporters found in this list probably reflects the conservative nature of our estimates. We studied the *hif-1*-independent, *vhl-1*-dependent gene set using enrichment analysis but no terms were significantly enriched.

Identification of non-classical epistatic interactions

hif-1(lf) has traditionally been viewed as existing in a genetic OFF state under normoxic conditions. However, our dataset indicates that 546 genes show altered expression when *hif-1* function is removed in normoxic conditions. Moreover, we observed positive correlations between *hif-1(lf)* β coefficients and *egl-9(lf)*, *vhl-1(lf)* and *rhy-1(lf)* β coefficients in spite of the negative regulatory relationships between these genes and *hif-1*. Such positive correlations could indicate a different relationship between these genes than has previously been reported, so we attempted to substantiate them through epistasis analyses.

To perform epistasis analyses, we first identified genes that exhibited violations of the canonical genetic model of the hypoxia pathway. To this end, we searched for genes that exhibited different behaviors between *egl-9(lf)* and *vhl-1(lf)*, or between *rhy-1(lf)* and *vhl-1(lf)* (we assume that all results from the *rhy-1(lf)* transcriptome reflect a complete loss of *egl-9* activity). We found 31 that satisfied this condition (see Fig. 10, Supplemental Table 4). Additionally, many of these genes exhibited a new kind of epistasis. Namely, *egl-9* was epistatic over *vhl-1*. Identification of a set of genes that have a consistent set of relationships between themselves suggests that we have identified a new aspect of the hypoxia pathway.
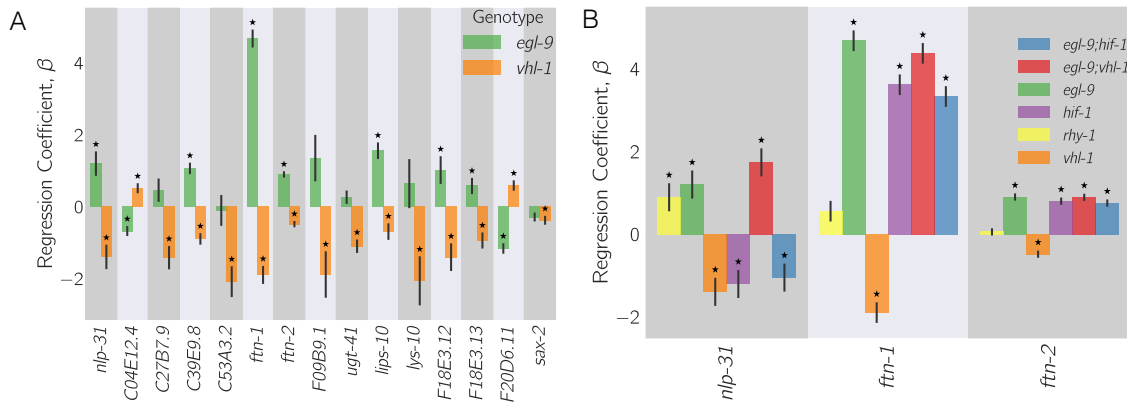

Figure 10. A. 27 genes in *C. elegans* exhibit non-classical epistasis in the hypoxia pathway, characterized by opposite effects on gene expression, relative to the wild-type, of of the *vhl-1(lf)* compared to *egl-9(lf)* (or *rhy-1(lf)*) mutants. Shown are a random selection of 15 the 27 genes for illustrative purposes. **B**. Representative genes showing that non-canonical epistasis shows a consistent pattern. *vhl-1(lf)* mutants have an opposite effect to *egl-9(lf)*, but *egl-9* remains epistatic to *vhl-1* and loss-of-function mutations in *hif-1* suppress the *egl-9(lf)* phenotype. Asterisks show β values significantly different from 0 relative to wild-type ($q < 10^{-1}$).

To illustrate this, we focused on three genes, *nlp-31*, *ftn-1* and *ftn-2*, which epistasis patterns that we felt reflected the population well. *ftn-1* and *ftn-2* are both described in the literature as genes that are responsive to mutations in the hypoxia pathway. Moreover, these genes have been previously described to have aberrant behaviors[45,46], specifically the opposite effects of *egl-9(lf)* and *vhl-1(lf)*. These studies showed that loss of *vhl-1(lf)* decreases expression of *ftn-1* and *ftn-2* using both RNAi and alleles, which allays concerns of strain-specific interference. Moreover, Ackerman and Gems (2012) showed that *vhl-1* is epistatic to *hif-1* for the *ftn-1* expression phenotype, and that loss of HIF-1 is associated with increased expression of *ftn-1*

and *ftn-2*. We observed that *hif-1* was epistatic to *egl-9*, and that *egl-9* and *hif-1* both promoted *ftn-1* and *ftn-2* expression.

Epistasis analysis of *ftn-1* and *ftn-2* expression reveals that *egl-9* is epistatic to *hif-1*; that *vhl-1* has opposite effects to *egl-9*, and that *vhl-1* is epistatic to *egl-9*. Analysis of *nlp-31* reveals similar relationships. *nlp-31* expression is decreased in *hif-1(lf)*, and increased in *egl-9(lf)*. However, *egl-9* is epistatic to *hif-1*. Like *ftn-1* and *ftn-2*, *vhl-1* has the opposite effect to *egl-9*, yet is epistatic to *egl-9*. We propose in the Discussion a model for how HIF-1 might regulate these targets.

HIF-1 in the cellular context

We identified the transcriptional changes associated with bioenergetic pathways in *C. elegans* by extracting from WormBase all genes associated with the tricarboxylic acid (TCA) cycle, the electron transport chain (ETC) and with the *C. elegans* GO term energy reserve. Previous research has described the effects of mitochondrial dysfunction in eliciting the hypoxia response[48], but transcriptional feedback from HIF-1 into bioenergetic pathways has not been as extensively in *C. elegans*, as in vertebrates (see, for example[32,28]). We also searched for the changes in ribosomal components and the proteasome, as well as for terms relating to immune response (see Fig 11).
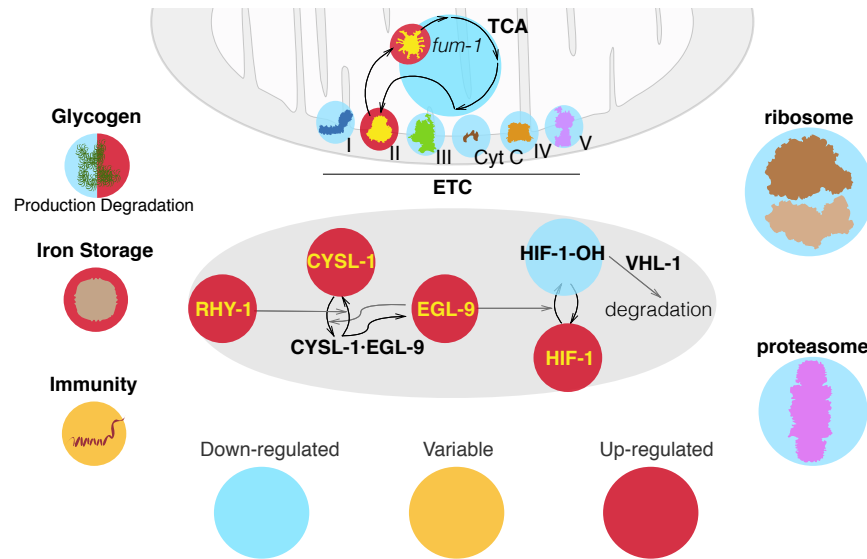

Figure 11. A graphic summary of the genome-wide effects of HIF-1 from our RNA-seq data.

Bioenergetic pathways

Our data shows that most of the enzymes involved in the TCA cycle and in the ETC are down-regulated when HIF-1 is induced in agreement with the previous literature[28]. However, the fumarase gene *fum-1* and the mitochondrial complex II stood out as notable exceptions to the trend, as they were up-regulated in every single genotype that causes deployment of the hypoxia response. FUM-1 catalyzes the reaction of fumarate into malate, and complex II catalyzes the reaction of succinate into fumarate. Complex II has been identified as a source of reserve respiratory capacity in neonatal rat cardiomyocytes previously[49]. We found two energy reserve genes that were down-regulated by HIF-1. *aagr-1* and *aagr-2*, which are predicted to function in glycogen catabolism[50]. Three distinct genes involved in energy reserve were up-regulated. These genes were *ogt-1*, which encodes O-linked GlcNac Transferase gene; *T04A8.7*, encoding an ortholog of human glucosidase, acid beta (GBA); and *T22F3.3*, encoding ortholog of human glycogen phosphorylase isozyme in the muscle (PYGM).

Protein synthesis and degradation

hif-1(lf) is also known to inhibit protein synthesis and translation in varied ways.[51]. Most reported effects of HIF-1 on the translation machinery are posttranslational, and no reports to date show transcriptional control of the ribosomal machinery in *C. elegans* by HIF-1. We used the WormBase Enrichment Suite Gene Ontology dictionary[43] to extract 143 protein-coding genes annotated as 'structural constituents of the ribosome' and we queried whether they were differentially expressed in our mutants. *egl-9(lf)*, *vhl-1(lf)*, *rhy-1(lf)* and *egl-9(lf)*;*vhl-1(lf)* showed differential expression of 91 distinct ribosomal constituents (not all constituents were detected in all genotypes). For every one of these genotypes, these genes were always down-regulated. In contrast, *hif-1(lf)* showed up-regulation of a single ribosomal constituent.

Next, we asked whether HIF-1 has any transcriptional effects on the proteasomal constituents; no such effects of HIF-1 on the proteasome have been reported in *C. elegans*. Out of 40 WormBase-annotated proteasomal constituents, we found 31 constituents that were differentially expressed in at least one of the four genotypes that induce a hypoxic response. Every gene we found was down-regulated in at least two out of the four genotypes we studied.

Discussion

The *C. elegans* hypoxia pathway can be reconstructed entirely from RNA-seq data

In this paper, we have shown that whole-organism transcriptomic phenotypes can be used to reconstruct genetic pathways and to discern previously overlooked or uncharacterized genetic interactions. We successfully reconstructed the hypoxia pathway, and inferred order of action (*rhy-1* activates *egl-9*, *egl-9* and *vhl-1* inhibit *hif-1*), and we were able to infer from transcriptome-wide epistasis measurements that *egl-9* exerts *vhl-1*-dependent and independent inhibition on *hif-1*.

HIF-1 and the cellular environment

In addition to reconstructing the pathway, our dataset allowed us to observe a wide variety of physiologic changes that occur as a result of the HIF-1-dependent hypoxia response. In particular, we observed down-regulation of most components of the TCA cycle and the mitochondrial electron transport chain with the exceptions of *fum-1* and the mitochondrial complex II. The mitochondrial complex II catalyzes the reaction of succinate into fumarate. In mouse embryonic fibroblasts, fumarate has been shown to antagonize HIF-1 prolyl hydroxylase domain (PHD) enzymes, which are orthologs of EGL-9[52]. If the inhibitory role of fumarate on PHD enzymes is conserved in *C. elegans*, upregulation of complex II by HIF-1 during hypoxia may increase intracellular levels of fumarate, which in turn could lead to artificially high levels of HIF-1 even after normoxia resumes. The increase in fumarate produced by the complex could be compensated by increasing expression of *fum-1*. Increased fumarate degradation allows *C. elegans* to maintain plasticity in the hypoxia pathway, keeping the pathway sensitive to oxygen levels.

Interpretation of the non-classical epistasis in the hypoxia pathway

The observation of almost 30 genes that exhibit a specific pattern of non-classical epistasis suggests the existence of previously undescribed aspects of the hypoxia pathway. Some of these non-classical epistases had been observed previously[45,46,44], but no satisfactory mechanism has been proposed to explain this biology.[46] and[45] suggest that HIF-1 integrates information on iron concentration in the cell to bind to the *ftn-1* promoter, but could not definitively establish a mechanism. It is unclear why deletion of *hif-1* induces *ftn-1* expression, deletion of *egl-9* also causes induction of *ftn-1* expression, but deletion of *vhl-1* removes this inhibition. Moreover,[44] have previously reported that certain genes important for the *C. elegans* immune response against pathogens reflect similar expression patterns. Their interpretation was that *swan-1*, which encodes a binding partner to EGL-9[53], is important for modulating HIF-1 activity in some manner. The lack of a conclusive double mutant analysis in this work means the role of SWAN-1 in modulation of HIF-1 activity remains to be demonstrated. Nevertheless, mechanisms that call for additional transcriptional

modulators become less likely given the number of genes with different biological functions that exhibit the same pattern.
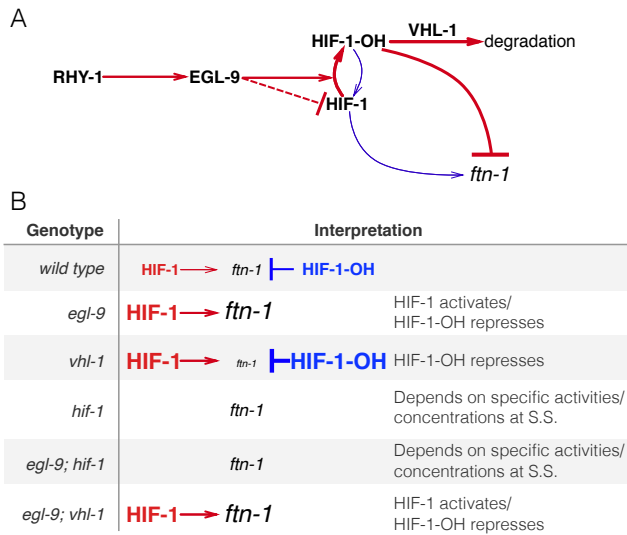

Figure 12. A hypothetical model showing a mechanism where HIF-1-hydroxyl antagonises HIF-1. **A**. Diagram showing that RHY-1 activates EGL-9. EGL-9 hydroxylates HIF-1 in an oxygen dependent fashion. Under normoxia, HIF-1 is rapidly hydroxylated and only slowly does hydroxylated HIF-1 return to its original state. EGL-9 can also inhibit HIF-1 in an oxygen-independent fashion. HIF-1 hydroxyl is rapidly degraded in a VHL-1 dependent fashion. In our model, HIF-1 and HIF-1 hydroxyl have opposing effects on transcription. The width of the arrows represents the rates under normoxic conditions. **B**. Table showing the effects of loss-of-function mutations on HIF-1 and HIF-1 hydroxyl activity, showing how this can potentially explain the behavior of *ftn-1* in each case. S.S = Steady-state.

One way to resolve this problem without invoking additional genes is to consider HIF-1 as a protein with both activating and inhibiting states. In fact, HIF-1 already exists in two states in *C. elegans*: unmodified HIF-1 and HIF-1-hydroxyl (HIF-1-OH). Under this model, HIF-1-hydroxyl antagonizes the effects of HIF-1 for certain genes like *ftn-1* or *nlp-31*. Loss of *vhl-1* stabilizes HIF-1-hydroxyl. A subset of genes that are sensitive to HIF-1-hydroxyl will be inhibited as a result of the increase in the amount of this species, in spite of loss of *vhl-1* function also increasing the level of non-hydroxylated HIF-1. On the other hand, *egl-9(lf)* selectively removes all HIF-1-hydroxyl, stimulating accumulation of HIF-1 and promoting gene activity. Whether deletion of *hif-1(lf)* is overall activating or inhibiting will depend on the relative activity of each protein state under normoxia (see Fig. 12).

Multiple lines of circumstantial evidence that HIF-1-hydroxyl plays a role in the functionality of the hypoxia pathway. First, HIF-1-hydroxyl is challenging to study genetically because no mimetic mutations are available with which to study the pure hydroxylated HIF-1 species. Second, although mutations in the Von-Hippel Landau gene stabilize the hydroxyl species, they also increase the quantity of non-hydroxylated HIF-1 by mass action. Finally, since HIF-1 is detected low levels in cells under normoxic conditions[54], total HIF-1 protein (unmodified HIF-1 plus HIF-1-hydroxyl) is often tacitly assumed to be vanishingly rare and therefore biologically inactive.

Our data show hundreds of genes that change expression in response to loss of *hif-1* under normoxic conditions. This establishes that there is sufficient total HIF-1 protein to be biologically active. Our analyses also revealed that *hif-1(lf)* shares positive correlations with *egl-9(lf)*, *rhy-1(lf)* and *vhl-1(lf)*, and that each of these genotypes also shows a secondary negative rank-ordered expression correlation with each other. These cross-patterns between all loss of function of inhibitors of HIF-1 and *hif-1(lf)* can be most easily explained if HIF-1-hydroxyl is biologically active.

A homeostatic argument can be made in favor of the activity of HIF-1-hydroxyl. At any point in time, the cell must measure the levels of multiple metabolites at once. The *hif-1*-dependent hypoxia response integrates information from O_2, α-ketoglutarate (2-oxoglutarate) and iron concentrations in the cell. One

way to integrate this information is by encoding it only in the effective hydroxylation rate of HIF-1 by   493
EGL-9. Then the dynamics in this system will evolve exclusively as a result of the total amount of HIF-1 in   494
the cell. Such a system can be sensitive to fluctuations in the absolute concentration of HIF-1[55]. Since the   495
absolute levels of HIF-1 are low in normoxic conditions, small fluctuations in protein copy-number represent   496
can represent a large fold-change in HIF-1 levels. These fluctuations would not be problematic for genes that   497
must be turned on only under conditions of severe hypoxia—presumably, these genes would be associated   498
with low affinity sites for HIF-1, so that they are only activated when HIF-1 levels are far above random   499
fluctuations.   500

For yet other sets of genes that must change expression in response to the hypoxia pathway, it may   501
not make as much sense to integrate metabolite information exclusively via EGL-9-dependent hydroxylation   502
of HIF-1. In particular, genes that may function to increase survival in mild hypoxia may benefit from   503
regulatory mechanisms that can sense minor changes in environmental conditions and which therefore benefit   504
from robustness to transient changes in protein copy number. Likewise, genes that are involved in iron or   505
α-ketoglutarate metabolism (such as *ftn-1*) may benefit from being able to sense, accurately, small and   506
consistent deviations from basal concentrations of these metabolites. For these genes, the information may   507
be better encoded by using HIF-1 and HIF-1-hydroxyl as an activator/repressor pair. Such circuits are known   508
to possess distinct advantages for controlling output in a manner that is robust to transient fluctuations in   509
the levels of their components[56,57].   510

Our RNA-seq data suggests that one of these atypical targets of HIF-1 may be RHY-1. Although *rhy-1*   511
does not exhibit non-classical epistasis, *hif-1(lf)* and *egl-9(lf) hif-1(lf)* both had increased expression levels   512
of *rhy-1*. We speculate that if *rhy-1* is controlled by both HIF-1 and HIF-1-hydroxyl, then this might imply   513
that HIF-1 regulates the expression of its pathway (and therefore itself) in a manner that is robust to total   514
HIF-1 levels.   515

Insights into genetic interactions from vectorial phenotypes   516

Here, we have described a set of straightforward methods that can be in theory applied to any vectorial   517
phenotype. Genome-wide methods afford a lot of information, but genome-wide interpretation of the results   518
is often extremely challenging. Each method has its own advantages and disadvantages. We briefly discuss   519
these methods, their uses and their drawbacks.   520

Principal component analysis is computationally tractable and clusters can often be visually detected   521
with ease. However, PCA can be misleading, especially when the dimensions represented do not explain a   522
very large fraction of the variance present in the data. In addition, principal dimensions are the product   523
of a linear combination of vectors, and therefore must be interpreted with extreme care. In this case, the   524
first principal dimension separated genotypes that increase HIF-1 protein levels from those that decrease it,   525
but this dimension is a mix of vectors of change in gene expression. Although PCA showed that there is   526
information hidden in these genotypes, it was not enough by itself to provide biological insight.   527

Whereas PCA operates on all genotypes simultaneously, correlation analysis is a pairwise procedure   528
that measures how predictable the gene expression changes are in a mutant given the vector of expression   529
changes in another. Like PCA, correlation analysis is easy and fast to perform. Unlike PCA, the product of   530
a correlation analysis is a single number with a straightforward interpretation. However, correlation analysis   531
is particularly sensitive to outliers. Although a common strategy is to rank-transform expression data to   532
mitigate outliers, rank-transformations do not remove the cross-patterns that appear when feedback loops   533
or other complex interactions are present between two genes. Such cross-patterns can still lead to vanishing   534
correlations if both patterns are equally strong. Therefore, correlation analyses must take into account the   535
possible existence of systematic outliers. Moreover, correlation values must be measured for both interactions   536
in cross-patterned rank plots. Weighted correlations could be informative for ordering genes along pathways.   537
A drawback of correlation analysis is that the number of pairwise comparisons that must be made increases   538
combinatorially, though strategies could be used to decrease the total number of effective comparisons.   539

Epistasis plots are a novel way to visualize epistasis in vectorial phenotypes. Here, we have shown how   540
an epistasis plot can be used to identify interactions between two single mutants and a double mutant. In   541
reality, epistasis plots can be generated for any set of measurements involving a set of N mutants and an   542
N-mutant genotype. Epistasis plots can accumulate an arbitrary number of points within them, possess a   543
rich structure that can be visualized and have straightforward interpretations for special slope values.   544

Another way to analyze epistasis is via general linear models (GLMs) that include interaction terms between two or more genes. In this way, GLMs can quantify the epistatic effect of an interaction on single genes. We and others[22,23] have previously used GLMs to identify gene sets that are epistatically regulated by two or more inputs. While powerful, GLMs suffer from the multiple comparison problem. Correcting for false positives using well-known multiple comparison corrections such as FDR[58] tends to increase false negative rates. Moreover, since GLMs attempt to estimate effect magnitudes for individual gene or isoform expression levels, they effectively treat each gene as an independent quantity, which prevents better estimation of the magnitude and direction of the epistasis between two genes.

Epistasis plots do not suffer from the multiple comparison problem because the number of tests performed is orders of magnitudes smaller than the number of tests performed by GLMs. Ideally, in an epistasis plot we need only perform 3 tests—rejection of additive, unbranched and suppressive null models—compared with the tens of thousands of tests that are performed in GLMs. Moreover, the magnitude of epistasis between two genes can be estimated using hundreds of genes, which greatly improves the statistical resolution of the epistatic coefficient. This increased resolution is important because the size and magnitude of the epistasis has specific consequences for the type of pathway that is expected.

Any quantitative use of genome-wide datasets requires a good experimental setup. Here, we have demonstrated that whole-organism RNA-seq can be used to dissect molecular pathways in exquisite detail when paired with experimental designs that are motivated by classical genetics. Much more research will be necessary to understand whether epistasis has different consequences in the microscopic realm of transcriptional phenotypes than in the macroscopic world that geneticists have explored previously. Our hope is that these tools, coupled with the classic genetics experimental designs, will reveal hitherto unknown aspects of genetics theory.

Methods

Nematode strains and culture

Strains used were N2 wild-type Bristol, CB5602 *vhl-1(ok161)*, CB6088 *egl-9(sa307) hif-1(ia4)*, CB6116 *egl-9(sa307);vhl-1(ok161)*, JT307 *egl-9(sa307)*, ZG31 *hif-1(ia4)*, RB1297 *rhy-1(ok1402)*. All lines were grown on standard nematode growth media (NGM) plates seeded with OP50 *E. coli* at 20°C (Brenner 1974).

RNA Isolation

Unsynchronized lines were grown on NGM plates at 20C and eggs harvested by sodium hypochlorite treatment. Eggs were plated on 6 to 9 6cm NGM plates with ample OP50 *E. coli* to avoid starvation and grown at 20°C. Worms were staged and harvested based on the time after plating, vulva morphology and the absence of eggs. Approximately 30–50 non-gravid young adults were picked and placed in 100μL of TE pH 8.0 at 4°C in 0.2mL PCR tubes. After settling and a brief spin in microcentrifuge approximately 80μL of TE (Ambion AM 9849) was removed from the top of the sample and individual replicates were snap frozen in liquid N2. These replicate samples were then digested with Proteinase K (Roche Lot No. 03115 838001 Recombinant Proteinase K PCR Grade) for 15min at 60° in the presence of 1% SDS and 1.25μL RNA Secure (Ambion AM 7005). RNA samples were then taken up in 5 Volumes of Trizol (Tri Reagent Zymo Research) and processed and treated with DNase I using Zymo MicroPrep RNA Kit (Zymo Research Quick-RNA MicroPrep R1050). RNA was eluted in RNase-free water and divided into aliquots and stored at -80°C. One aliquot of each replicate was analyzed using a NanoDrop (Thermo Fisher) for impurities, Qubit for concentration and then analyzed on an Agilent 2100 BioAnalyzer (Agilent Technologies). Replicates were selected that had RNA integrity numbers (RIN) equal or greater than 9.0 and showed no evidence of bacterial ribosomal bands, except for the ZG31 mutant where one of three replicates had a RIN of 8.3.

Library Preparation and Sequencing

10ng of quality checked total RNA from each sample was reverse-transcribed into cDNA using the Clontech SMARTer Ultra Low Input RNA for Sequencing v3 kit (catalog #634848) in the SMARTSeq2 protocol [59]. RNA was denatured at 70°C for 3 minutes in the presence of dNTPs, oligo dT primer and spiked-in

quantitation standards (NIST/ERCC from Ambion, catalog #4456740). After chilling to 4°C, the first-strand reaction was assembled using the LNA TSO primer described in[59], and run at 42°C for 90 minutes, followed by denaturation at 70°C for 10 minutes. The entire first strand reaction was then used as template for 13 cycles of PCR using the Clontech v3 kit. Reactions were cleaned up with 1.8X volume of Ampure XP SPRI beads (catalog #A63880) according to the manufacturer's protocol. After quantification using the Qubit High Sensitivity DNA assay, a 3ng aliquot of the amplified cDNA was run on the Agilent HS DNA chip to confirm the length distribution of the amplified fragments. The median value for the average cDNA lengths from all length distributions was 1076bp. Tagmentation of the full length cDNA for sequencing was performed using the Illumina/Nextera DNA library prep kit (catalog #FC-121–1030). Following Qubit quantitation and Agilent BioAnalyzer profiling, the tagmented libraries were sequenced. Libraries were sequenced on Illumina HiSeq2500 in single read mode with the read length of 50nt to an average depth of 15 million reads per sample following manufacturer's instructions. Base calls were performed with RTA 1.13.48.0 followed by conversion to FASTQ with bcl2fastq 1.8.4. Spearman correlation of the transcripts per million (TPM) for each genotype showed that every pairwise correlation within genotype was > 0.9.

Read Alignment and Differential Expression Analysis

We used Kallisto to perform read pseudo-alignment and performed differential analysis using Sleuth. We fit a general linear model for a transcript t in sample i:

$$y_{t,i} = \beta_{t,0} + \beta_{t,genotype} \cdot X_{t,i} + \beta_{t,batch} \cdot Y_{t,i} + \epsilon_{t,i} \tag{1}$$

where $y_{t,i}$ are the logarithm transformed counts; $\beta_{t,genotype}$ and $\beta_{t,batch}$ are parameters of the model, and which can be interpreted as biased estimators of the log-fold change; $X_{t,i}, Y_{t,i}$ are indicator variables describing the conditions of the sample; and $\epsilon_{t,i}$ is the noise associated with a particular measurement.

Genetic Analysis, Overview

Genetic analysis of the processed data was performed in Python 3.5. Our scripts made extensive use of the Pandas, Matplotlib, Scipy, Seaborn, Sklearn, Networkx, Bokeh, PyMC3, and TEA libraries[60,61,62,63,64,65,66,42,67]. Our analysis is available in a Jupyter Notebook[68]. All code and required data (except the raw reads) are available at https://github.com/WormLabCaltech/mprsq along with version-control information. Our Jupyter Notebook and interactive graphs for this project can be found at https://wormlabcaltech.github.io/mprsq/. Raw reads were deposited in the Short Read Archive under the study accession number SRP100886.

Weighted Correlations

Pairwise correlations between transcriptomes where calculated by first identifying the set of differentially expressed genes (DEGs) common to both transcriptomes under analysis. DEGs were then rank-ordered according to their regression coefficient, β. Bayesian robust regressions were performed using a Student-T distribution. Bayesian analysis was performed using the PyMC3 library[64] (`pm.glm.families.StudenT` in Python). If the correlation has an average value > 1, the correlation coefficient was set to 1.

Weights were calculated as the proportion of genes that were < 1.5 standard deviations away from the primary regression out of the entire set of shared DEGs for each transcriptome.

Epistasis Analysis

For a double mutant X^-Y^-, we used the single mutants X^- and Y^- to find expected value of the coefficient for a double mutant under an additive model for each isoform i. Specifically,

$$\beta_{\text{Add},i} = \beta_{X,i} + \beta_{Y,i}. \tag{2}$$

Next, we find the difference, Δ_i, between the observed double mutant expression coefficient, $\beta_{XY,\text{Obs},i}$, and the predicted expression coefficient under an additive model for each isoform i.

To calculate the transcriptome-wide epistasis coefficient, we plotted $(\beta_{\text{Add},i}, \Delta_i)$ and found the line of best fit using orthogonal distance regression using the `scipy.odr` package in Python. We performed non-parametric bootstrap sampling of the ordered tuples with replacement using 5,000 iterations to generate a probability distribution of slopes of best fit.

There are as many models as epistatic relationships. For quantitative phenotypes, epistatic relationships (except synthetic interactions) can be generally expressed as:

$$\beta_{XY} = \sum_{g \in G} \lambda_g \beta_g, \tag{3}$$

where P_i is the quantitative phenotype belonging to the genotype i; G is the set of single mutants $\{X, Y\}$ that make up the double mutant, XY; and λ_g is the contribution of the phenotype P_g to P_{XY}. Additive interactions between genes are the result of setting $\lambda_g = 1$. All other relationships correspond to setting $\lambda_X = 0$, $\lambda_Y = 1$ or $\lambda_X = 1$, $\lambda_Y = 0$.

A given epistatic interaction can be simulated by predicting the double mutant phenotype under that interaction and re-calculating the y-coordinates. The recalculated y-coordinates can then be used to predict the possible epistasis coefficients for the cases where X is epistatic over Y, and Y is epistatic over X.

To select between theoretical models, we implemented an approximate Bayesian Odds Ratio. We defined a free-fit model, M_1, that found the line of best fit for the data:

$$P(\alpha \,|M_1, D) \propto \prod_{(x_i, y_i, \sigma_i) \in D} \exp \frac{(y_i - \alpha \cdot x_i)^2}{2\sigma_i} \cdot (1 + \alpha^2)^{-3/2}, \tag{4}$$

where α is the slope of the model to be determined, x_i, y_i were the x- and y-coordinates of each point respectively, and σ_i was the standard error associated with the y-value. We minimized the negative logarithm of equation 4 to obtain the most likely slope given the data, D (`scipy.optimize.minimize` in Python). Finally, we approximated the odds ratio as:

$$OR = \frac{P(D \,|\alpha^*, M_1) \cdot (2\pi)^{1/2} \sigma_{\alpha^*}}{P(D \,|M_i)}, \tag{5}$$

where α^* is the slope found after minimization, σ_α^* is the standard deviation of the parameter at the point α^* and $P(D \,|M_i)$ is the probability of the data given the parameter-free model, M_i.

Enrichment Analysis

Tissue, Phenotype and Gene Ontology Enrichment Analysis were carried out using the WormBase Enrichment Suite for Python[43,42].

Author Contributions:

Competing Interests:

The authors declare they have no conflicts of interest.

References

1. Huang, L. S. & Sternberg, P. W. Genetic dissection of developmental pathways. *WormBook : the online review of* C. elegans *biology* 1–19 (2006).

2. Phillips, P. C. Epistasis—the essential role of gene interactions in the structure and evolution of genetic systems. *Nat Rev Genet* **9**, 855–867 (2008).

3. Mortazavi, A., Williams, B. A., McCue, K., Schaeffer, L. & Wold, B. Mapping and quantifying mammalian transcriptomes by RNA-Seq. *Nature Methods* **5**, 621–628 (2008).

4. Metzker, M. L. Sequencing technologies - the next generation. *Nature reviews. Genetics* **11**, 31–46 (2010).

5. Patro, R., Mount, S. M. & Kingsford, C. Sailfish enables alignment-free isoform quantification from RNA-seq reads using lightweight algorithms. *Nature biotechnology* **32**, 462–464 (2014).

6. Bray, N. L., Pimentel, H. J., Melsted, P. & Pachter, L. Near-optimal probabilistic RNA-seq quantification. *Nature biotechnology* **34**, 525–7 (2016).

7. Patro, R., Duggal, G., Love, M. I., Irizarry, R. A. & Kingsford, C. Salmon provides accurate, fast, and bias-aware transcript expression estimates using dual-phase inference. *bioRxiv* 021592 (2016).

8. Pimentel, H. J., Bray, N. L., Puente, S., Melsted, P. & Pachter, L. Differential analysis of RNA-Seq incorporating quantification uncertainty. *bioRxiv* 058164 (2016).

9. Trapnell, C. *et al.* Differential analysis of gene regulation at transcript resolution with RNA-seq. *Nature biotechnology* **31**, 46–53 (2013).

10. Singer, M. *et al.* A Distinct Gene Module for Dysfunction Uncoupled from Activation in Tumor-Infiltrating T Cells. *Cell* **166**, 1500–1511.e9 (2016).

11. Shalek, A. K. *et al.* Single-cell transcriptomics reveals bimodality in expression and splicing in immune cells. *Nature* **498**, 236–40 (2013).

12. Schwarz, E. M., Kato, M. & Sternberg, P. W. Functional transcriptomics of a migrating cell in *Caenorhabditis elegans. Proceedings of the National Academy of Sciences of the United States of America* **109**, 16246–51 (2012).

13. Van Wolfswinkel, J. C., Wagner, D. E. & Reddien, P. W. Single-cell analysis reveals functionally distinct classes within the planarian stem cell compartment. *Cell Stem Cell* **15**, 326–339 (2014).

14. Scimone, M. L., Kravarik, K. M., Lapan, S. W. & Reddien, P. W. Neoblast specialization in regeneration of the planarian *Schmidtea mediterranea. Stem Cell Reports* **3**, 339–352 (2014).

15. Hughes, T. R. *et al.* Functional Discovery via a Compendium of Expression Profiles. *Cell* **102**, 109–126 (2000).

16. Van Driessche, N. *et al.* Epistasis analysis with global transcriptional phenotypes. *Nature Genetics* **37**, 471–477 (2005).

17. Brem, R. B., Yvert, G., Clinton, R. & Kruglyak, L. Genetic Dissection of Transcriptional Regulation in Budding Yeast. *Science* **296** (2002).

18. Schadt, E. E. *et al.* Genetics of gene expression surveyed in maize, mouse and man. *Nature* **422**, 297–302 (2003).

19. Li, Y. *et al.* Mapping Determinants of Gene Expression Plasticity by Genetical Genomics in *C. elegans. PLoS Genetics* **2**, e222 (2006).

20. King, E. G., Sanderson, B. J., McNeil, C. L., Long, A. D. & Macdonald, S. J. Genetic Dissection of the *Drosophila melanogaster* Female Head Transcriptome Reveals Widespread Allelic Heterogeneity. *PLoS Genetics* **10**, e1004322 (2014).

21. Adamson, B. *et al.* A Multiplexed Single-Cell CRISPR Screening Platform Enables Systematic Dissection of the Unfolded Protein Response. *Cell* **167**, 1867–1882.e21 (2016).

22. Dixit, A. *et al.* Perturb-Seq: Dissecting Molecular Circuits with Scalable Single-Cell RNA Profiling of Pooled Genetic Screens. *Cell* **167**, 1853–1866.e17 (2016).

23. Angeles-Albores, D. *et al.* Transcriptomic Description of an Endogenous Female State in *C. elegans*. *bioRxiv* (2016).

24. Epstein, A. C. R. *et al.* *C. elegans* EGL-9 and mammalian homologs define a family of dioxygenases that regulate HIF by prolyl hydroxylation. *Cell* **107**, 43–54 (2001).

25. Shen, C., Shao, Z. & Powell-Coffman, J. A. The *Caenorhabditis elegans rhy-1* Gene Inhibits HIF-1 Hypoxia-Inducible Factor Activity in a Negative Feedback Loop That Does Not Include *vhl-1*. *Genetics* **174**, 1205–1214 (2006).

26. Shao, Z., Zhang, Y. & Powell-Coffman, J. A. Two Distinct Roles for EGL-9 in the Regulation of HIF-1-mediated gene expression in *Caenorhabditis elegans*. *Genetics* **183**, 821–829 (2009).

27. Jiang, H., Guo, R. & Powell-Coffman, J. A. The *Caenorhabditis elegans* hif-1 gene encodes a bHLH-PAS protein that is required for adaptation to hypoxia. *Proceedings of the National Academy of Sciences of the United States of America* **98**, 7916–7921 (2001).

28. Semenza, G. L. Hypoxia-inducible factors in physiology and medicine. *Cell* **148**, 399–408 (2012).

29. Loenarz, C. *et al.* The hypoxia-inducible transcription factor pathway regulates oxygen sensing in the simplest animal, *Trichoplax adhaerens*. *EMBO reports* **12**, 63–70 (2011).

30. Jiang, B. H., Rue, E., Wang, G. L., Roe, R. & Semenza, G. L. Dimerization, DNA binding, and transactivation properties of hypoxia-inducible factor 1. *The Journal of biological chemistry* **271**, 17771–17778 (1996).

31. Powell-Coffman, J. A., Bradfield, C. A. & Wood, W. B. *Caenorhabditis elegans* Orthologs of the Aryl Hydrocarbon Receptor and Its Heterodimerization Partner the Aryl Hydrocarbon Receptor Nuclear Translocator. *Proceedings of the National Academy of Sciences* **95**, 2844–2849 (1998).

32. Semenza, G. L., Roth, P. H., Fang, H. M. & Wang, G. L. Transcriptional regulation of genes encoding glycolytic enzymes by hypoxia-inducible factor 1. *The Journal of Biological Chemistry* **269**, 23757–63 (1994).

33. Bishop, T. *et al.* Genetic Analysis of Pathways Regulated by the von Hippel-Lindau Tumor Suppressor in *Caenorhabditis elegans*. *PLoS Biology* **2** (2004).

34. Shen, C., Nettleton, D., Jiang, M., Kim, S. K. & Powell-Coffman, J. A. Roles of the HIF-1 hypoxia-inducible factor during hypoxia response in *Caenorhabditis elegans*. *Journal of Biological Chemistry* **280**, 20580–20588 (2005).

35. Bellier, A., Chen, C. S., Kao, C. Y., Cinar, H. N. & Aroian, R. V. Hypoxia and the hypoxic response pathway protect against pore-forming toxins in *C. elegans*. *PLoS Pathogens* **5** (2009).

36. Huang, L. E., Arany, Z., Livingston, D. M. & Franklin Bunn, H. Activation of hypoxia-inducible transcription factor depends primarily upon redox-sensitive stabilization of its α subunit. *Journal of Biological Chemistry* **271**, 32253–32259 (1996).

37. Kaelin, W. G. & Ratcliffe, P. J. Oxygen Sensing by Metazoans: The Central Role of the HIF Hydroxylase Pathway. *Molecular Cell* **30**, 393–402 (2008).

38. Ma, D. K., Vozdek, R., Bhatla, N. & Horvitz, H. R. CYSL-1 Interacts with the O_2-Sensing Hydroxylase EGL-9 to Promote H_2S-Modulated Hypoxia-Induced Behavioral Plasticity in *C. elegans*. *Neuron* **73**, 925–940 (2012).

39. Yeung, K. Y. & Ruzzo, W. L. Principal component analysis for clustering gene expression data. *Bioinformatics (Oxford, England)* **17**, 763–774 (2001).

40. Park, E. C. *et al.* Hypoxia regulates glutamate receptor trafficking through an HIF-independent mechanism. *The EMBO Journal* **31**, 1618–1619 (2012).

41. Powell-Coffman, J. A. Hypoxia signaling and resistance in *C. elegans*. *Trends in Endocrinology and Metabolism* **21**, 435–440 (2010).

42. Angeles-Albores, D., N. Lee, R. Y., Chan, J. & Sternberg, P. W. Tissue enrichment analysis for *C. elegans* genomics. *BMC Bioinformatics* **17**, 366 (2016).

43. Angeles-Albores, D., Lee, R. Y., Chan, J. & Sternberg, P. W. Phenotype and gene ontology enrichment as guides for disease modeling in C. elegans. *bioRxiv* (2017).

44. Luhachack, L. G. *et al.* EGL-9 Controls *C. elegans* Host Defense Specificity through Prolyl Hydroxylation-Dependent and -Independent HIF-1 Pathways. *PLoS Pathogens* **8**, 48 (2012).

45. Ackerman, D. & Gems, D. Insulin/IGF-1 and hypoxia signaling act in concert to regulate iron homeostasis in *Caenorhabditis elegans*. *PLoS Genetics* **8** (2012).

46. Romney, S. J., Newman, B. S., Thacker, C. & Leibold, E. A. HIF-1 regulates iron homeostasis in *Caenorhabditis elegans* by activation and inhibition of genes involved in iron uptake and storage. *PLoS Genetics* **7** (2011).

47. Semenza, G. L. Hypoxia-inducible factor 1: Regulator of mitochondrial metabolism and mediator of ischemic preconditioning. *Biochimica et Biophysica Acta - Molecular Cell Research* **1813**, 1263–1268 (2011).

48. Lee, S. J., Hwang, A. B. & Kenyon, C. Inhibition of respiration extends *C. elegans* life span via reactive oxygen species that increase HIF-1 activity. *Current Biology* **20**, 2131–2136 (2010).

49. Pfleger, J., He, M. & Abdellatif, M. Mitochondrial complex II is a source of the reserve respiratory capacity that is regulated by metabolic sensors and promotes cell survival. *Cell Death and Disease* **6**, 1–14 (2015).

50. Sikora, J. *et al.* Bioinformatic and biochemical studies point to AAGR-1 as the ortholog of human acid α-glucosidase in *Caenorhabditis elegans*. *Molecular and Cellular Biochemistry* **341**, 51–63 (2010).

51. Brugarolas, J. *et al.* Regulation of mTOR function in response to hypoxia by REDD1 and the TSC1/TSC2 tumor suppressor complex. *Genes and Development* **18**, 1–12 (2004).

52. Sudarshan, S. *et al.* Fumarate hydratase deficiency in renal cancer induces glycolytic addiction and hypoxia-inducible transcription factor 1α stabilization by glucose-dependent generation of reactive oxygen species. *Mol Cell Biol* **29**, 4080–4090 (2009).

53. Shao, Z., Zhang, Y., Ye, Q., Saldanha, J. N. & Powell-Coffman, J. A. *C. elegans* SWAN-1 binds to EGL-9 and regulates HIF-1- mediated resistance to the bacterial pathogen *Pseudomonas aeruginosa* PAO1. *PLoS Pathogens* **6**, 91–92 (2010).

54. Wang, G. L. & Semenza, G. L. Characterization of hypoxia-inducible factor 1 and regulation of DNA binding activity by hypoxia. *The Journal of Biological Chemistry* **268**, 21513–8 (1993).

55. Goentoro, L., Shoval, O., Kirschner, M. W. & Alon, U. The Incoherent Feedforward Loop Can Provide Fold-Change Detection in Gene Regulation. *Molecular Cell* **36**, 894–899 (2009).

56. Hart, Y., Antebi, Y. E., Mayo, A. E., Friedman, N. & Alon, U. Design principles of cell circuits with paradoxical components. *Proceedings of the National Academy of Sciences of the United States of America* **109**, 8346–8351 (2012).

57. Hart, Y. & Alon, U. The Utility of Paradoxical Components in Biological Circuits. *Molecular Cell* **49**, 213–221 (2013).

58. Storey, J. D. & Tibshirani, R. Statistical significance for genomewide studies. *Proceedings of the National Academy of Sciences of the United States of America* **100**, 9440–5 (2003).

59. Picelli, S. *et al.* Full-length RNA-seq from single cells using Smart-seq2. *Nature protocols* **9**, 171–81 (2014).

60. Bokeh Development Team. Bokeh: Python library for interactive visualization (2014).

61. McKinney, W. pandas: a Foundational Python Library for Data Analysis and Statistics. *Python for High Performance and Scientific Computing* 1–9 (2011).

62. Oliphant, T. E. SciPy: Open source scientific tools for Python. *Computing in Science and Engineering* **9**, 10–20 (2007).

63. Pedregosa, F. *et al.* Scikit-learn: Machine Learning in Python. *Journal of Machine Learning Research* **12**, 2825–2830 (2012).

64. Salvatier, J., Wiecki, T. & Fonnesbeck, C. Probabilistic Programming in Python using PyMC. *PeerJ Computer Science* **2**, 1–24 (2015).

65. Van Der Walt, S., Colbert, S. C. & Varoquaux, G. The NumPy array: A structure for efficient numerical computation. *Computing in Science and Engineering* **13**, 22–30 (2011).

66. Hunter, J. D. Matplotlib: A 2D graphics environment. *Computing in Science and Engineering* **9**, 99–104 (2007).

67. Waskom, M. *et al.* seaborn: v0.7.0 (January 2016) (2016).

68. Pérez, F. & Granger, B. IPython: A System for Interactive Scientific Computing Python: An Open and General- Purpose Environment. *Computing in Science and Engineering* **9**, 21–29 (2007).